13th International Symposium on Turbulence and Shear Flow Phenomena (TSFP13)
Montreal, Canada, June 25–28, 2024

TURBULENT BOUNDARY LAYER SCALE INTERACTIONS IN THE PRESENCE OF A FREESTREAM CYLINDER WAKE

Guangyao Cui
Faculty of Aerospace Engineering
Technion Israel Institute of Technology
Haifa, 32000 Israel

Alexey Zhelebovskiy
Faculty of Aerospace Engineering
Technion Israel Institute of Technology
Haifa, 32000 Israel

Ian Jacobi
Faculty of Aerospace Engineering
Technion Israel Institute of Technology
Haifa, 32000 Israel
ijacobi@technion.ac.il

ABSTRACT

Coherent motions from a free-stream cylinder wake were shown to induce phase-modulation behavior in scale-interactions inside a neighboring turbulent boundary layer. Wake/boundary layer interactions occur in a wide range of engineering problems, and they reorganize the structure of the near wall flow in ways that substantially impact skin friction and heat transfer properties. In this experimental study, we quantified the boundary layer reorganization due to a free-stream cylinder wake in terms of spatial phase-lag relationships between large- and small-scale motions within the boundary layer, which were shown to be highly affected by the structure of coherent motions in the wake. By averaging the scale interaction spatial-lag with respect to the period of the wake vortex shedding, we identified a phase-modulation process between large- and small-scale features which may potentially be exploited for fine-tuning future control strategies. Steady rolling-wall actuators on the cylinder were also used to modify the wake shear layers in order to show how the phase-modulation and minimal phase-lag condition between scales can be manipulated.

BACKGROUND

Understanding the interactions between large- and small-scale coherent structures in turbulence is critical in developing efficient control strategies for turbulent flows. Bandyopadhyay & Hussain (1984) first proposed a filter-based decomposition of an instantaneous flow measurement into a large-scale signal and an envelope of small-scale fluctuations. This decomposition has been subsequently used to infer the existence of amplitude modulation relationships between the scales (Mathis *et al.*, 2009). Marusic *et al.* (2010) showed how a linear model for scale interactions can be used to predict near-wall behavior from outer-flow sensors, which can then be exploited for active drag reduction (Abbassi *et al.*, 2017). Most of the research on this scale-interaction problem has been focused on canonical flows — primarily zero-pressure gradient boundary layers and channels — where the relationships between large- and small-scales appear largely consistent, as expressed via phase or skewness measures. The scale interaction problem has also been explored in non-canonical flows, in the presence of favorable or adverse pressure gradients (Harun *et al.*, 2013), high levels of free-stream turbulence (Dogan *et al.*, 2016), and downstream of roughness transitions (Li *et al.*, 2023), all of which modestly shift the observed spatial lag between the large- and small-scale fluctuations.

To further interrogate these scale-interactions, artificial large-scale motions (LSMs) have been injected into a turbulent boundary layer by flow actuation to observe their subsequent relationship with small-scale fluctuations. Whether these artificial LSMs were generated via oscillations at the wall (Jacobi & McKeon, 2017) or via plasma actuators in the free-stream (Ranade *et al.*, 2019) or from inside the boundary layer (Lozier *et al.*, 2023), they were observed to organize the small scales very similarly to the organization imposed by natural LSMs, albeit with shifts in the spatial lags separating the different scales. While the motivation for artificially injecting VLSMs into the boundary layer was the development of practical control schemes, there is also an entire class of wall-bounded flows that involve the natural injection of highly structured LSMs: boundary layers in the presence of periodic, free-stream wake shedding. The interaction between a bluff-body wake and a wall is important to turbomachinery, wind farms, heat exchangers, and a variety of fluid-structure interaction problems (Bearman & Zdravkovich, 1978; Squire, 1989). And, depending on the Reynolds number, Re, the wake naturally contains coherent LSMs in the form of shed vortices that can penetrate the neighboring boundary layer, initiate transition in laminar flows, or reorganize the near-wall structure of turbulent flows. De Souza *et al.* (1999) have shown that these wake LSMs can exert substantial influence on both drag and heat transfer, although the precise mechanisms have not been explained in the context of the influence of large-scale structures on small scales. Therefore, wake/boundary-layer flows are an ideal test case for examining the unsteady injection of large-scale motions into a boundary layer of significant engineering importance.

In this study, we describe the interactions between large- and small-scale coherent motions in a turbulent boundary layer exposed to a freestream cylinder wake in order to explain the influence of periodic coherent structures on the scale interac-

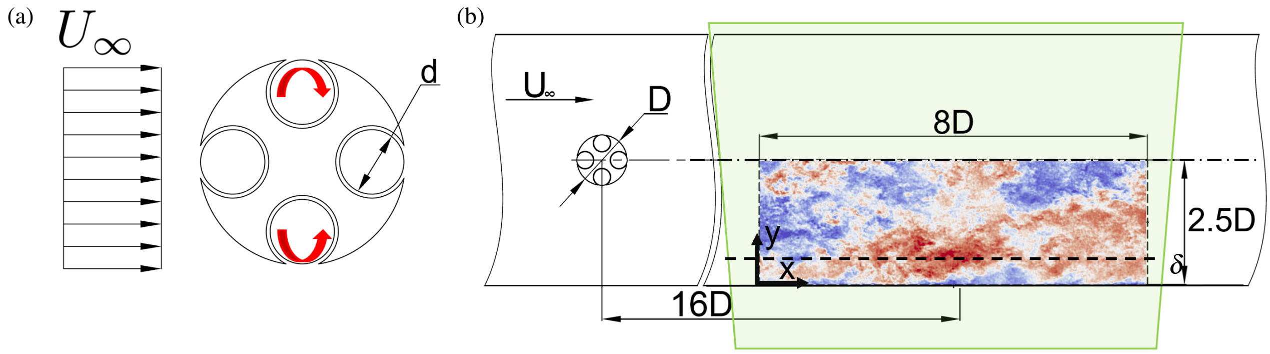

Figure 1: (a) Sketch of the actuated cylinder embedded with four freely rotating rollers. Only the two marked rollers were used for the actuation experiments. (b) The experimental layout with the cylinder oriented spanwise (z). The x-averaged boundary layer thickness, δ, is marked by the dashed line.

tion problem near the wall. In particular, we identify a phase-modulation process between large- and small-scales due to the wake, show how this produces a minimum spatial lag between the scales, and utilize steady flow actuators on the cylinder to modify the minimum spatial lag behavior.

EXPERIMENTAL METHOD

The turbulent scale interactions in the wake/boundary layer problem were studied experimentally in a high speed water tunnel facility (test section length 2m; square cross-section dimension $a = 0.2$m). A modified cylinder with four equal-spaced, azimuthal, 'rolling wall' actuators was suspended at the upstream side of the test section at mid-plane. To accommodate the actuators, the cylinder diameter was quite large at $D = 40$mm which created an appreciable blockage in the flow field, $D/a = 0.2$. The rolling walls were embedded cylinders ('rollers') with diameter $d = 13.5$mm. The rollers were independently rotated by four motors, although in the present study only the top and bottom rollers, situated near the natural separation points, were utilized, as shown in figure 1(a).

Measurements of the turbulent boundary layer were made along the lower tunnel wall at the downstream end of the test section using two-component, planar, particle image velocimetry (PIV) at the central streamwise/wall-normal (x/y) plane that was time-resolved for large-scales only. The field of view started 12D downstream of the cylinder, and extended for approximately 8D in the streamwise direction and from the wall to the tunnel centerline in the wall-normal direction. More details about the water tunnel and PIV measurements in the tunnel can be found in Cui *et al.* (2022). Figure 1(b) shows the overall layout of the experiment.

Experiments were performed at a cylinder Reynolds number, $\mathrm{Re}_D = U_\infty D/\nu \approx 10^5$, where the freestream velocity U_∞ was measured at the inlet of the test section, and the kinematic viscosity is ν. Due to the presence of the cylinder wake, the boundary layer downstream was highly distorted, and its thickness, δ, was defined as the location of the local maximum velocity, which occurs where the shear layer of the wake intersects with the intermittent edge of the boundary layer. Three experimental scenarios were observed: the boundary layer downstream of an unactuated freestream cylinder, the boundary layer downstream of an actuated cylinder, and a canonical boundary layer without the presence of a cylinder wake (at similar Reynolds number, Re_δ, to the wake-modified boundary layers). The canonical boundary layer without the cylinder had $\mathrm{Re}_\tau = u_\tau\delta/\nu \approx 2150$ where the friction velocity u_τ was obtained by a modified Clauser fit. For each scenario, 10 PIV recordings were made at 0.4KHz with two high speed cameras (Phantom VEO-340L and VEO-440L), each at spatial resolutions of 2560×1600 pixels. Table 1 lists the physical dimensions associated with the experiments and the corresponding measurement resolutions in dimensional and outer units.

Figure 2 shows wake/boundary-layer profiles of (a) the mean velocity and (b) the turbulence intensity for different streamwise locations downstream of the cylinder, in gray. The red line corresponds to the profile for the canonical boundary layer (without a cylinder). Figure 2(c) shows the temporal spectral map of the boundary layer as a function of frequency, f, across its wall-normal extent, y/δ, averaged over the streamwise direction. The cylinder sheds large-scale vortices with a Strouhal number of $\mathrm{St}_0 = fD/U_\infty \approx 0.22$ (which is slightly higher than the classical result due to the blockage effect of the tunnel). Contour lines from the same spectral map of the canonical boundary layer (converted from the spatial spectrum via Taylor's hypothesis due to low temporal resolution) are superimposed for reference, and show that the vortex shedding in the wake exerts a significant influence on the natural LSMs in the boundary layer itself, largely overwhelming them.

SCALE INTERACTION ANALYSIS

In order to examine the relationship between the large- and small-scale features of the wake-modified boundary layer, the velocity fields were decomposed following the general procedure of Bandyopadhyay & Hussain (1984) in which the Reynolds-decomposed, fluctuating streamwise velocity signal, u, was low-pass filtered to obtain a large-scale signal, u_L, and the remainder of the fluctuating signal, $u_S = u - u_L$, was enveloped by the Hilbert transform (Mathis *et al.*, 2009) and then rectified to obtain an envelope signal, $\mathbf{E}\{u_S\}$, that was compared with the large-scale scale signal via correlation techniques. However, unlike most of the previous studies on scale interactions, we performed the scale decomposition and filtering in the spatial domain in order to obtain the resulting spatial large- and small-scale fields as a function of time. By preserving the time-dependence of the scale decomposition, we were then able to observe how the scale interactions evolved in time, and, in particular, how they varied over an average period of the wake oscillation.

The spatial instantaneous velocity fields were filtered using a one-dimensional, 3rd-order, zero-shift, Butterworth filter for each wall-normal location, independently, with spatial cut-

	Re_δ	$U_\infty(m/s)$	$\delta(m)$	$u_\tau(m/s)$	L_x/δ	L_y/δ	$\Delta x/\delta$	$\Delta t U_\infty/\delta$	δ/D
Boundary Layer (BL)	5.7×10^4	2.39	0.024	0.093	11.9	3.7	0.019	0.25	0.58
Wake-Modified BL	5.1×10^4	2.30	0.022	-	14.5	4.5	0.021	0.26	0.55
Actuated Wake-Mod. BL	4.1×10^4	2.30	0.018	-	17.7	5.5	0.025	0.32	0.45

Table 1: Key physical and measurement parameters in the experiment: free streamwise velocity, U_∞, measured at the test section inlet; boundary layer thickness, δ; friction velocity, u_τ; streamwise field-of-view, L_x/δ; wall-normal field-of-view, L_y/δ; spatial resolution, $\Delta x/\delta$; temporal resolution, $\Delta t U_\infty/\delta$; ratio of boundary layer thickness to cylinder diameter, δ/D.

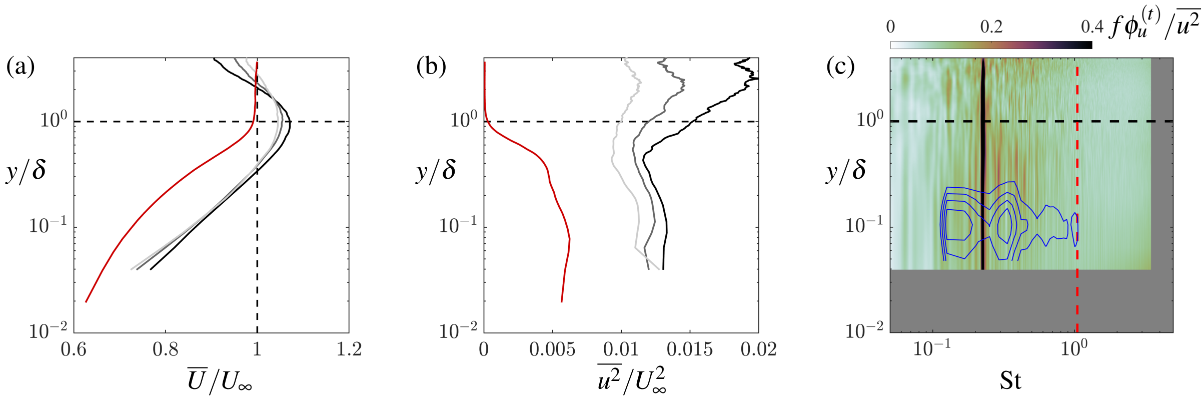

Figure 2: The boundary-layer wake profiles at different streamwise locations, x, for (a) the mean velocity, $\overline{U}$ and (b) the streamwise Reynolds stress calculated from $u = U - \overline{U}$. Lighter gray with increasing streamwise location: $x/D = 12, 16, 20$. (c) Pre-multiplied temporal energy spectral density across wall-normal positions, y; the temporal-equivalent filtering cut-off is marked in red; blue contour levels from the canonical boundary layer.

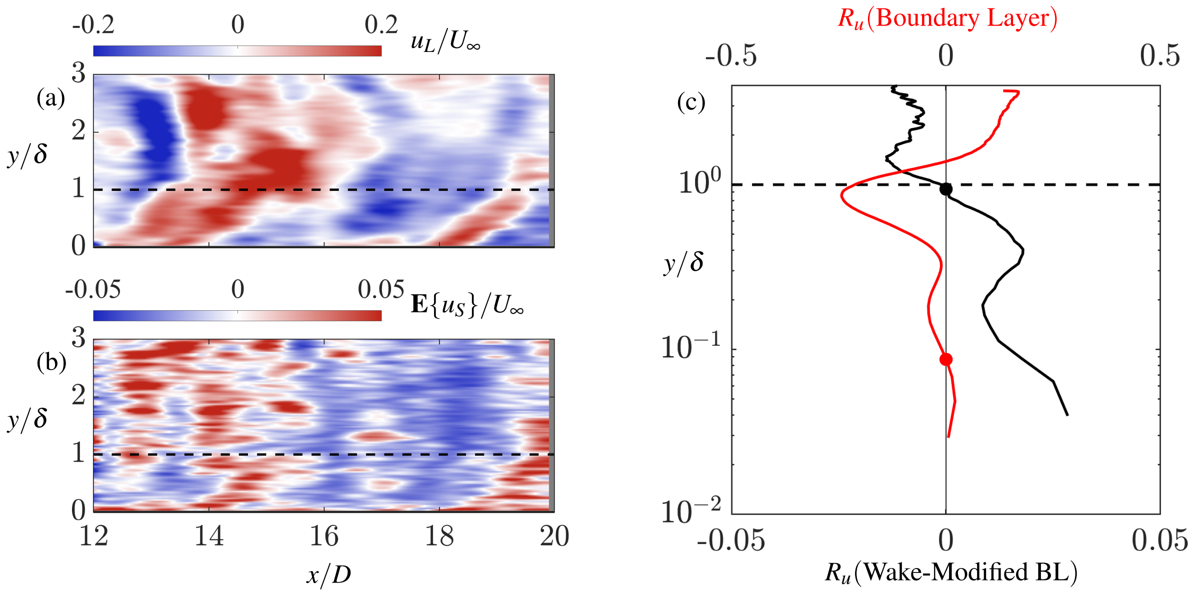

Figure 3: A single frame of the spatially filtered, instantaneous, streamwise velocity field showing (a) the large-scale signal, u_L, and (b) the small-scale envelope, $\mathbf{E}\{u_S\}$, with mean removed. The black dashed line is boundary layer. (c) The correlation coefficient, R_u, for the canonical boundary layer (red) and the wake-modified boundary layer (black).

off wavelength, $\lambda_c \approx D$. The spatial filter cut-off is equivalent to a temporal cutoff of $\mathrm{St}_c = 5\,\mathrm{St}_0$ using the free-stream velocity, U_∞, and Taylor's hypothesis and is marked as the red dashed line in figure 2(c). Figure 3(a) shows the large-scale signal from a representative instantaneous snapshot of the flow, and figure 3(b) shows the corresponding envelope of the small-scale fluctuations (with mean removed). The downstream inclination of the structures is clear in both filtered signals.

The relationship between the large- and small-scale structures has been characterized by a cross-correlation function (Bandyopadhyay & Hussain, 1984) and a correlation coefficient (Mathis *et al.*, 2009). The spatial cross-correlation function for the streamwise velocity, $r_u(\Delta x, y, t)$, for a single pair

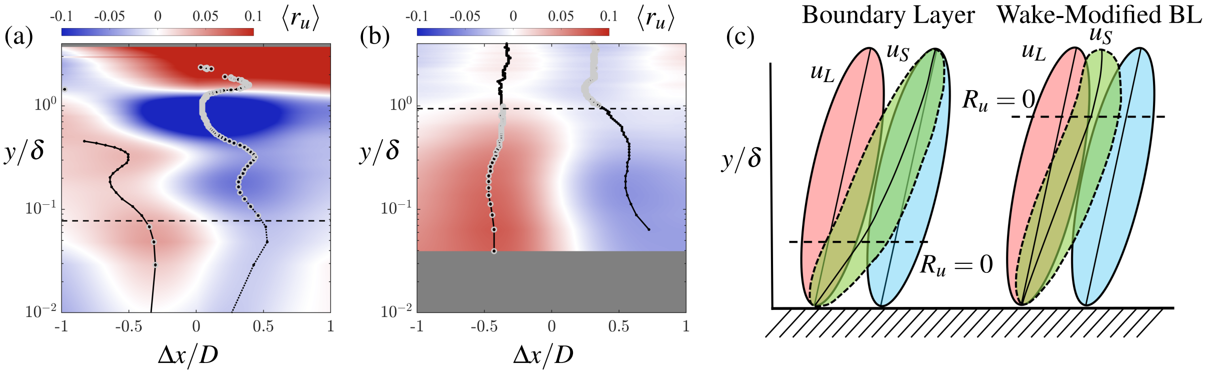

Figure 4: The ensemble-averaged cross-correlation function, $\langle r_u\rangle(\Delta x, y)$, for (a) the canonical boundary layer and (b) the wake-modified boundary layer. The local extrema for each y-location are marked in black points; the absolute extremum at each height is circled in white. The location of the jump between a positive extremum near the wall and a negative extremum away from the wall corresponds to the location where $R_u = 0$. (c) Cartoons of the relative spatial orientation of the large scales (red and blue for positive and negative modes) and small-scale envelope (green).

of fields at time, t, was defined as

$$r_u(\Delta x, y, t) = \frac{\overline{u_L(x,y,t)\ \mathbf{E}\{u_S\}(x+\Delta x, y, t)}}{\left\langle \overline{u_L^2} \right\rangle^{1/2} \left\langle \overline{\mathbf{E}\{u_S\}^2} \right\rangle^{1/2}}, \qquad (1)$$

where $\overline{(\cdot)}$ indicates averaging over x and $\langle\cdot\rangle$ indicates averaging over t, and $\langle\overline{u_L^2}\rangle^{1/2}$ and $\langle\overline{\mathbf{E}\{u_S\}^2}\rangle^{1/2}$ are the global root mean square (rms) values of the two filtered velocity fields for each y-location. Ensemble averaging the cross-correlation function over all t yields $\langle r_u\rangle(\Delta x, y)$, which is equivalent to the global cross-correlation function used by Bandyopadhyay & Hussain (1984). Evaluating the global cross-correlation function for lag $\Delta x = 0$ yields the correlation coefficient, $R_u(y) = \langle r_u\rangle(0, y)$ used in Mathis *et al.* (2009).

Figure 3(c) shows the correlation coefficient as a function of wall-normal location for the canonical boundary layer (red) and the wake-modified boundary layer (black). As seen in previous studies, the coefficient is positive near the wall, crosses zero and is then negative far from the wall. Mathis *et al.* (2009) associated the zero-crossing location for the canonical boundary layer with the location of the outer peak of turbulent spectral energy associated with LSMs, situated in the middle of the log layer, and that is consistent with the current measurements, with a zero-crossing around $y/\delta \approx 0.09$. However, for the wake-modified boundary layer, the zero-crossing shifts outward to where the wake shear layer intersects the edge of the boundary layer, at around $y/\delta \approx 0.94$. This shift indicates that the large-scale features of the wake shear layer completely overwhelm the natural LSMs of the boundary layer itself, thereby reorganizing the structure of the amplitude modulation between scales.

Figure 4 shows the full maps of the cross-correlation function, $\langle r_u\rangle(\Delta x, y)$, for (a) the canonical boundary layer and (b) the wake-modified boundary layer downstream of the unactuated cylinder. The peaks of the cross-correlation indicate the dominant spatial phase-lag between the large- and small-scale signals, $\Delta x(y)$. Jacobi & McKeon (2013) interpreted this lag in terms of the relative spatial orientation of the large- and small-scales, illustrated schematically in figure 4(c). The canonical boundary layer shows an increasing spatial lag, with the small-scale envelope leading the large-scales, and the $R_u = 0$ location corresponding to an approximate lag of a quarter of the dominant wavelength (i.e. a phase-lag of $-\pi/2$). The wake-modified boundary layer displays a much more gradual increase in the spatial lag, where the quarter-wavelength lead of the small-scale envelope occurs only at the outer edge of the boundary layer itself. The presence of the wake structures therefore brought the large- and small-scale envelopes closer together (over most of the boundary layer thickness) compared to the flow without the wake. Moreover, the small spatial lag beyond the edge of the boundary layer indicates a distortion of the scale envelopes, generating an upstream inclination due to the presence of the wake shear layer. Here we illustrate that distortion in the small-scale envelope only, for simplicity; the PIV spatial resolution makes it difficult to assess whether the distortion also occurs in the large-scales.

PHASE MODULATION BEHAVIOR

The cylinder Reynolds number was quite modest ($\mathrm{Re}_D \approx 10^5$) resulting in highly periodic wake shedding with a prominent spectral peak shown in figure 2(c). Therefore, the scale-interaction behavior inside the neighboring boundary layer was studied in a phase-locked sense as it varied over a well-defined period of wake-shedding. To perform the phase-averaging, first the y-averaged, large-scale vertical velocity signal, $\langle v_L(x,t)\rangle$, was obtained via temporal filtering of the fluctuating velocity field at a frequency cut-off, (U_∞/D). The spatial correlation coefficient, $R_v(t)$, between this signal and a synthetic spatial signal, $\sin[2\pi x/(D/\mathrm{St}_0)]$, was then calculated for each time, t. This process eliminated x without naively averaging over the streamwise direction. Then the peaks of the $R_v(t)$ signal were identified and $n = 31$ phases were assigned between the peaks in order to obtain a phase signal, $\phi(t)$, that recorded the discrete phase for each t, which was used for phase-averaging.

Using the phase signal, the phase-averaged cross-correlation function, $r_u(\Delta x, y, \phi)$, was calculated from the local cross-correlation functions, $r_u(\Delta x, y, t)$, at each time. Then the phase-averaged spatial lag, $\Delta x(y, \phi)$ was calculated from the cross-correlation peaks. We found that $\Delta x(y, \phi)$ oscillated periodically about the global spatial lag, $\langle\Delta x(y)\rangle$, which was obtained by tracing along the cross-correlation peaks in figure 4(b). Figure 5 illustrates the averaged v_L signal over time (red), which was used to phase-lock the local cross-correlation functions for phase-averaging, in order to obtain the phase-

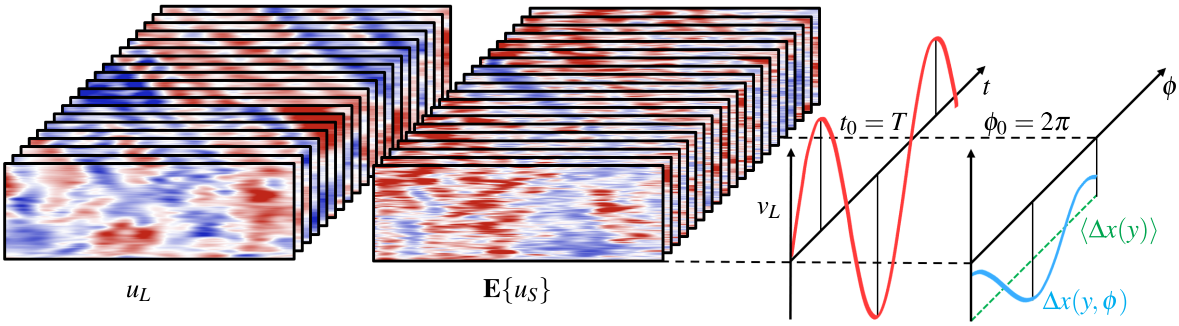

Figure 5: A schematic illustration of the phase-locked lag calculation. A phase signal (red) based on the filtered wall-normal fluctuation was used to tag each of the pairs of velocity fields, u_L and $\mathbf{E}\{u_S\}$, with a phase $\phi(t)$. The local cross-correlation function, $r_u(\Delta x, y, t)$, was then phase averaged, and the spatial lag, $\Delta x(y, \phi)$, was obtained.

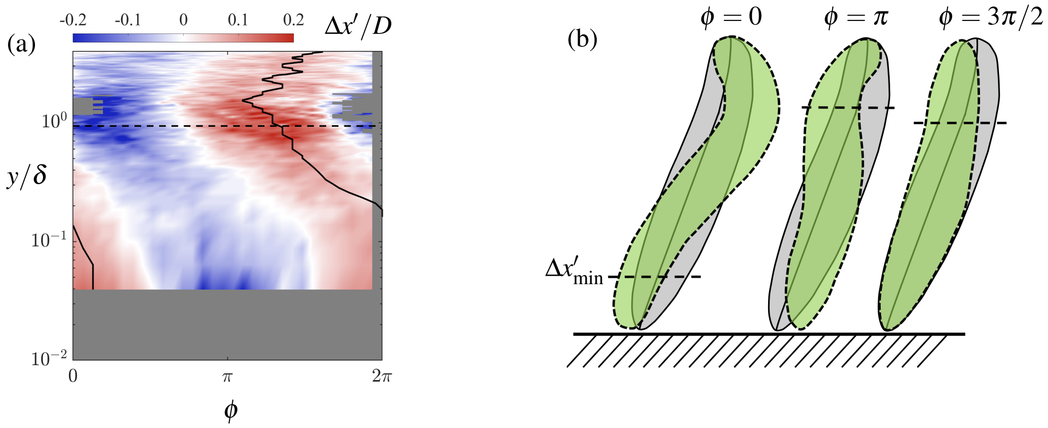

Figure 6: (a) Phase averaged relative spatial lag, $\Delta x'(y, \phi)$ showing the phase modulation behavior. The black line marks the minimal spatial lag, where the large- and small-scale envelopes are spatially closest. (b) A sketch of the globally-averaged small-scale envelope (gray) and phase-dependent envelope (green) varying over a period, where the y-location of minimal spatial lag, $\Delta x'_{\mathrm{min}}$, varies with phase.

averaged spatial lag, $\Delta x(y, \phi)$ (blue), which varies periodically about the global spatial lag, $\langle \Delta x(y) \rangle$ (green), over a period of oscillation.

The oscillation of the spatial lag between scales over time provides the first evidence that the present authors are aware of for the existence of phase-modulation in unsteady, turbulent scale interactions. Not only do the large scales modulate the amplitude of the small-scale fluctuations as reported by Mathis *et al.* (2009), but the spatial phase-lag between the scales is itself modulated by the large-scale, periodic oscillations in an unsteady flow.

We examined the phase modulation more clearly by subtracting the global lag from the phase-averaged lag to define a relative lag, $\Delta x'(y, \phi) = \Delta x(y, \phi) - \langle \Delta x(y) \rangle$, as shown in figure 6(a). The phase modulation behavior is quite prominent and varies with wall-normal location. The peak of the red region (black line) indicates the lowest magnitude (most positive) change in the spatial lag, $\Delta x'_{\mathrm{min}}$, i.e. the phase during the oscillation in which the large- and small-scale envelopes are spatially closest to each other. The y-location of minimal spatial lag varies with phase. Therefore, for a fixed wall-normal location, we can speculate that certain phases of the dominant period may be more amenable to flow actuation of small-scales via large-scales since the two envelopes are spatially closer during those phases. The phase dependence of the small-scale envelope is illustrated schematically over a period in figure 6(b), where the gray scale represents the globally averaged envelope of small-scale mode and the green represents the phase-dependent envelope of the small-scales. However, this cartoon could be drawn equivalently with respect to phase-dependent variations in the large-scales, as noted above.

ACTUATED CYLINDER WAKE

In light of the speculation above that the minimal spatial lag condition may be a useful target for future flow control, we considered how that minimal spatial lag condition could be modified by actuating the cylinder in order to reorganize the shear layers of the wake. The rolling wall surfaces on the top and bottom of the cylinder were operated with a tangential velocity ratio of $\alpha = u_i/U_\infty = 0.7$, which led to a flatter wake defect profile, with higher velocity in the core of the wake, and a thinner boundary layer at the wall.

Figure 7(a) shows the global correlation map for the boundary layer downstream of the actuated cylinder. The location of $R_u = 0$ shifted closer to the wall, within the bound-

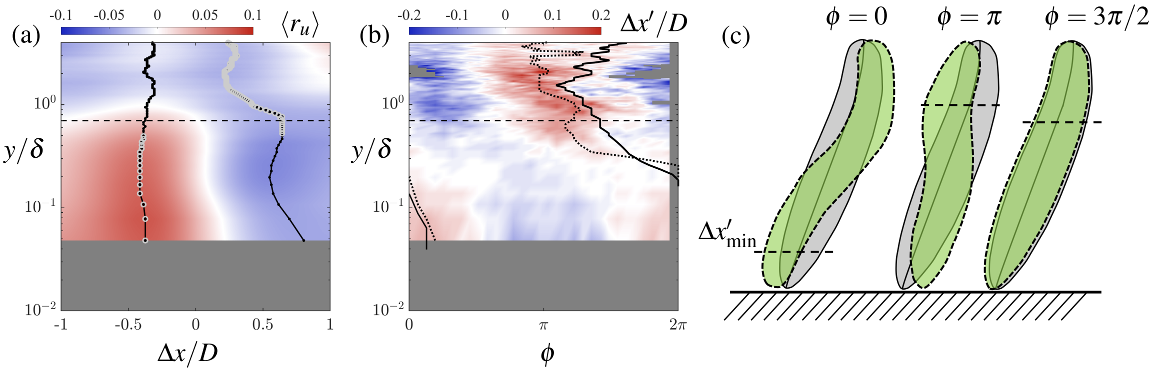

Figure 7: Spatial lag modifications due to actuation of the wake: (a) the global cross correlation map; (b) the phase-averaged spatial lag between scales, where the dashed line corresponds to the minimal lag condition (solid line is for the unactuated case). (c) Cartoon illustrating the change in minimal lag due to actuation.

ary layer, as opposed to the unactuated case where the $R_u = 0$ occurred at the outer edge of the boundary layer. This shift suggests that the large, wake oscillations tend to penetrate the boundary layer itself due to the actuation.

Figure 7(b) shows the phase-averaged, relative spatial lag $\Delta x'$ for the actuated wake, where the minimal spatial lag is marked (dotted line), for comparison with the minimal spatial lag for the unactuated wake (solid line). The change to the shear layer results in a shift in the phase location where the minimal spatial lag occurs (for fixed y), indicating that steady modification of the flow field is a potential tool for adjusting the receptivity of periodic flows to phase-targeted actuation. Figure 7(c) illustrates schematically how the steady wake actuation can shift the relative spatial lag between scales over the course of an oscillatory cycle.

CONCLUSIONS

The shedding of large-scale vortices in a cylinder wake provided a natural, periodic, free-stream forcing to a boundary layer that was shown to significantly reorganize the scale interactions between large- and small-scale motions. We utilized spatial filtering to separate the scales while preserving the time-dependence of the scale interactions. By calculating the phase-averaged cross-correlation between the large- and small-scale signals over the dominant period of wake vortex shedding, we identified a phase-modulation component to the scale interactions. The phase modulation means that the envelope of small-scale motions is spatially closer to the corresponding large scales during specific phases of the oscillation cycle, and these minimal spatial lag occurrences may be useful for designing future control schemes. Finally, we utilized steady surface actuation on the cylinder to modify the shear layers in the wake and thereby influence the phase-modulation behavior.

ACKNOWLEDGEMENTS

The authors gratefully acknowledge the support of the U.S. National Science Foundation and the U.S.-Israel Binational Science Foundation (NSF-BSF grant 2020698).

REFERENCES

Abbassi, M. R., Baars, W. J., Hutchins, N. & Marusic, I. 2017 Skin-friction drag reduction in a high-Reynolds-number turbulent boundary layer via real-time control of large-scale structures. *Int. J. Heat and Fluid Flow* **67**, 30–41.

Bandyopadhyay, P. R. & Hussain, A. K. M. F. 1984 The coupling between scales in shear flows. *Phys. of Fluids* **27** (9), 2221–2228.

Bearman, P. W. & Zdravkovich, M. M. 1978 Flow around a circular cylinder near a plane boundary. *J. Fluid Mech.* **89** (1), 33–47.

Cui, G., Ruhman, I. & Jacobi, I. 2022 Spatial detection and hierarchy analysis of large-scale particle clusters in wall-bounded turbulence. *J. Fluid Mech.* **942**, 1–28.

De Souza, F., Delville, J., Lewalle, J. & Bonnet, J. P. 1999 Large scale coherent structures in a turbulent boundary layer interacting with a cylinder wake. *Expt. Thermal and Fluid Sci.* **19** (4), 204–213.

Dogan, E., Hanson, R. E. & Ganapathisubramani, B. 2016 Interactions of large-scale free-stream turbulence with turbulent boundary layers. *J. Fluid Mech.* **802**, 79–107.

Harun, Z., Monty, J. P., Mathis, R. & Marusic, I. 2013 Pressure gradient effects on the large-scale structure of turbulent boundary layers. *J. Fluid Mech.* **715**, 477–498.

Jacobi, I. & McKeon, B. J. 2013 Phase relationships between large and small scales in the turbulent boundary layer. *Expts. in Fluids* **54**, 1481.

Jacobi, I. & McKeon, B. J. 2017 Phase-relationships between scales in the perturbed turbulent boundary layer. *J. Turbulence* **18** (12), 1120–1143.

Li, Mogeng, Baars, Woutijn J., Marusic, Ivan & Hutchins, Nicholas 2023 Quantifying inner-outer interactions in non-canonical wall-bounded flows. *Phys. Rev. Fluids* **8**, 084602.

Lozier, Mitchell, Thomas, Flint O. & Gordeyev, Stanislav 2023 Experimental investigation of turbulent boundary layer dynamics via active manipulation of large-scale structures. *Int. J. Heat and Fluid Flow* **103**, 109194.

Marusic, I., Mathis, R. & Hutchins, N. 2010 Predictive Model for Wall-Bounded Turbulent Flow. *Science* **329** (July), 193–197.

Mathis, R., Hutchins, N. & Marusic, I. 2009 Large-scale amplitude modulation of the small-scale structures in turbulent boundary layers. *J. Fluid Mech.* **628**, 311–337.

Ranade, P., Duvvuri, S., McKeon, B., Gordeyev, S., Christensen, K. & Jumper, E. J. 2019 Turbulence amplitude amplification in an externally forced, subsonic turbulent boundary layer. *AIAA J.* **57** (9), 3838–3850.

Squire, L. C. 1989 Interactions between wakes and boundary-layers. *Progress in Aero. Sci.* **26** (3), 261–288.